AIIM

Association for Information and Image Management

1100 Wayne Avenue, Suite 1100
Silver Spring, Maryland 20910
301/587-8202

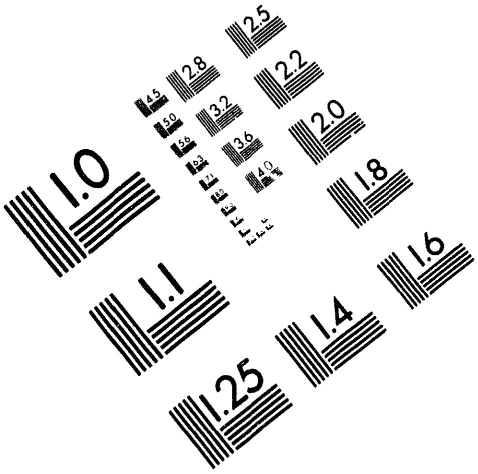

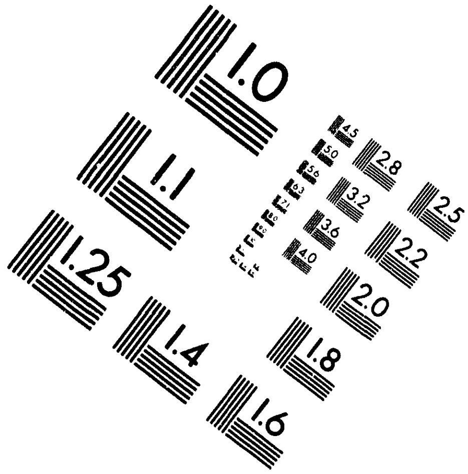

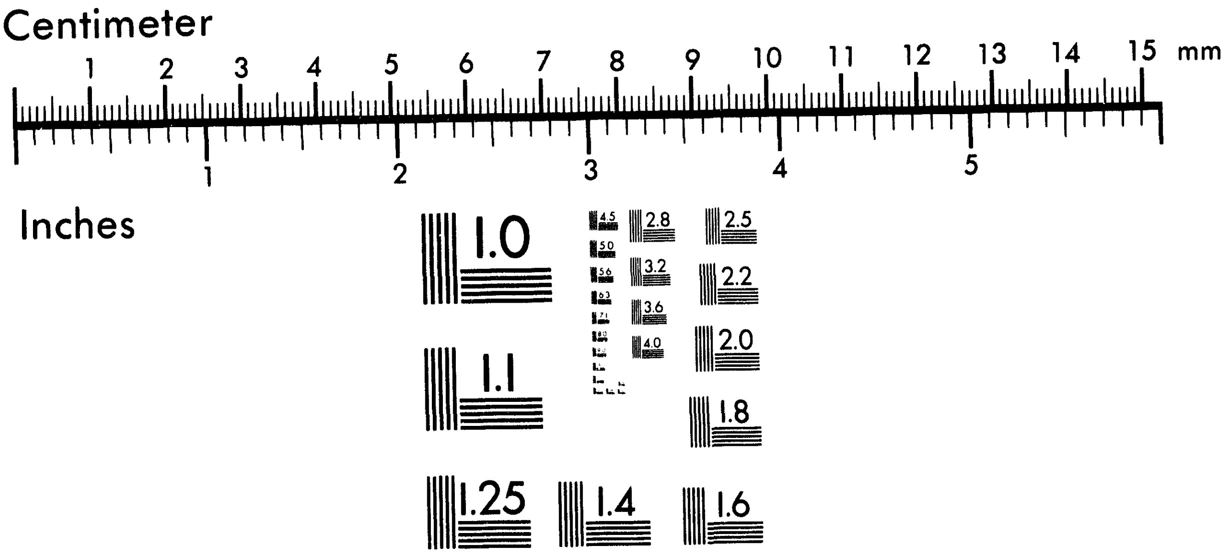

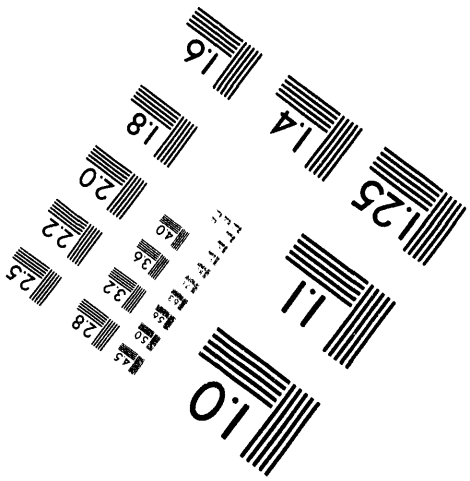

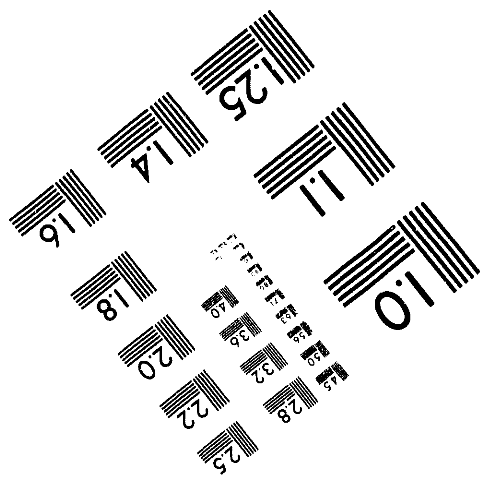

MANUFACTURED TO AIIM STANDARDS
BY APPLIED IMAGE, INC.

1 of 1

·2

LA-SUB--94-112

FINAL REPORT

for

THERMAL BLOOMING EXPERIMENTS

Subcontract Number
9-X29-D4357-1

May 1990

submitted to
UNIVERSITY OF CALIFORNIA
LOS ALAMOS NATIONAL LABORATORY
P. O. Box 990
Los Alamos, NM 87545

by
NORTH EAST RESEARCH ASSOCIATES, INC.
800 West Cummings Park, Suite 4900
Woburn, MA 01801

THERMAL BLOOMING EXPERIMENTS

1.0 INTRODUCTION

The goals of this program were to design an experiment for determining the effect of stimulated thermal Brillouin scattering (STBS) on single pulse laser propagation and to establish the ability of both a wave optics code and of linearized theory to predict the results of the experiment accurately. The second goal is particularly important because no experimental verification of analytical tools currently in use for single pulse high power laser propagation is available.

When a high power laser propagates through the atmosphere, a small fraction of the laser energy is absorbed, creating acoustic waves that may move a significant distance transverse to the propagation direction during the pulse. Such waves lead to the well-known t^3-blooming refractive-index variations. When such blooming is sufficiently strong, the induced refractive-index alters the intensity profile of the beam farther along the propagation path. This altered intensity profile induces a somewhat different refractive-index profile that may reinforce the path-integrated t^3 blooming. This self-enhancement may be called near-forward stimulated thermal Brillouin scattering (STBS).

The design effort described here was carried out much like the proposed experimental program, which calls for the interaction of experimental work with analytical theory and with a wave optics code, A linearized theory of STBS was developed. Results from this theory were compared to output from a wave optics propagation code for several well defined sets of operating conditions. Once good agreement between theory and code simulation was obtained for these test conditions, the theory was used to define an operating regime for a laboratory scale thermal blooming experiment that would provide information relevant to high power laser propagation. A conceptual design for this experiment was then generated and, finally, an experimental set-up, including diagnostics, was proposed.

Section 2.0 of this report discusses the linearized theory for STBS and Section 3.0 contains the comparison between theory and simulation. The conceptual design is presented in Section 4.0 and the recommended experiment set-up in Section 5.0.

2.0 LINEARIZED THEORY OF TRANSIENT LASER HEATING

The theoretical techniques used here to obtain results for STBS have previously been applied to the case of steady-state thermal blooming with considerable success. The term steady-state in this context refers to the regime where time scales are sufficiently long that nearly complete acoustic relaxation has occurred. In this regime, the main source of thermal blooming is then stimulated thermal Rayleigh scattering (STRS). For the current application, a term governing acoustic relaxation must be added to the equation describing the refractive index perturbation.

2.1 Basic Equations

The basic equation for the medium perturbation is

$$\frac{\partial}{\partial t}\left(\nabla_\perp^2 - \frac{1}{v_0^2}\frac{\partial^2}{\partial t^2}\right) s = -\frac{(\gamma-1)}{\gamma p_0}\,\alpha\,\nabla_\perp^2\, I \qquad (1)$$

where s is the relative medium perturbation $\delta\rho/\rho_0$, v_0 is the acoustic velocity and t is the time.

$\nabla_\perp$ and $\nabla_\perp^2$ are the gradient and Laplacian, respectively, transverse to the propagation direction z, γ is the ratio of specific heats c_p/c_v, p_0 is the ambient pressure, α is the absorption coefficient, and I is the laser intensity.

Now, the evolution of the electric field, E, also must be described. To do this, we use the paraxial equation. The equation of motion for light waves is then:

$$\left[\partial_z + \frac{\nabla_\perp^2}{2ik_0}\right] E = -ik_0\,\delta n\, E \qquad (2)$$

where $\delta n = (n_0-1)\,\delta\rho/\rho_0$ is the induced refractive index variation, and k_0 is the optical wavenumber. The electric field can be written $E = \sqrt{I}\, e^{\,i\phi}$ where I is the intensity and ϕ is the phase. We will assume that the intensity and phase can be decomposed into two parts,

one describing a unperturbed plane wave and the other small scale perturbations.

$$I = I_0 (1 + \delta I)$$
$$\phi = \phi_0 + \delta\phi \tag{3}$$

If the preceding expressions are substituted in eq. (2) and linearized about the unperturbed plane wave, the following equations result.

$$\partial_z \delta\phi - \frac{\nabla_\perp^2}{2k_0} \delta I = k_0 \delta n \tag{4}$$

$$\partial_z \delta I + \frac{\nabla_\perp^2}{2k_0} \delta\phi = 0 \tag{5}$$

Substituting the Fourier transforms for the intensity and phase:

$$\delta I = \int \exp(-ik\cdot x)\, \delta\tilde{I}(k)\, dk^2 \tag{6}$$

and

$$\delta\phi = \int \exp(-ik\cdot x)\, \delta\tilde{\phi}(k)\, dk^2 \tag{7}$$

one obtains

$$\partial_z \delta\tilde{\phi} + \frac{k^2}{2k_0} \delta\tilde{I} = k_0 \delta\tilde{n} \tag{8}$$

$$\partial_z \delta\tilde{I} - \frac{k^2}{2k_0} \delta\tilde{\phi} = 0 \tag{9}$$

Simplifying notation by dropping the tilde's ($\delta\tilde{I} \rightarrow \delta I$, $\delta\tilde{\phi} \rightarrow \delta\phi$), and changing the propagation variable to the dimensionless variable $\xi = k^2 z/2k_0$, one obtains for each transverse Fourier component:

$$\partial_\xi \delta I - \delta\phi = 0 \tag{10}$$

$$\partial_\xi \delta\phi + \delta I = \beta \delta n \tag{11}$$

where $\beta = \left(2k_0/k\right)^2/2$.

Similarly for the refractive-index variations,

$$\delta n = (n_0-1)\,\tilde{s}\,(k) \tag{12}$$

one obtains the following linearized equation of motion

$$\partial_t \left[\partial^2 + (v_0|k|)^2\right] \delta n = v_0|k|^2 \Gamma I_0\, \delta I \tag{13}$$

where $\Gamma = 2\,(n_0-1)\,(\gamma-1)\,\alpha/\gamma p_0$. Now, one may normalize the time variable to the dimensionless time $\tau = \Gamma I_0 \beta t$ and simplify the notation by writing

$$\mu = v_0 k/\Gamma I_0 \beta \tag{14}$$

One then obtains the following dimensionless version of Eq. (13):

$$\partial_\tau \left(\partial_\tau^2 + \mu^2\right) \partial n = -\mu^2 \frac{\delta I}{\beta} \tag{15}$$

Now we have three equations, (10), (11) and (15), in three unknowns, δn, $\delta\phi$, and δI. Two of these unknowns may be eliminated to obtain a simplified equation of motion.

To eliminate the phase perturbation $\delta\phi$ one may differentiate Eq. (10) and use Eq. (11) to eliminate $\partial_\xi \delta\phi$. One obtains

$$\left(\partial_\xi^2 + 1\right) \delta I = \beta\, \delta n \tag{16}$$

Applying the $(\partial_\xi^2 + 1)$ operator to both sides of Eq. (15) and substituting $\beta\, \delta n$ for the right-hand side of the resulting equation leads to the following result:

$$\left(\partial_\xi^2 + 1\right) \left(\partial_\tau^2 + \mu^2\right) \partial_\tau(\delta n) = -\mu^2\, \delta n \tag{17}$$

This linear partial differential equation is the central result of this effort. To make this equation more relevant to the situation of interest, set $\delta n = \delta n_B + \delta n_T$, where δn_B is the blooming contribution, and δn_T is the turbulence contribution. The temporal operator

operating on the turbulence contribution yields nearly zero because the turbulence is assumed to obey the frozen-flow hypothesis. Thus Eq. (17) may be simplified to give an inhomogeneous equation for the blooming contribution:

$$\left\{ \left(\partial_\xi^2 + 1\right)\left(\partial_\tau^2 / \mu^2 + 1\right)\partial_\tau + 1 \right\} \delta n_B = \delta n_T \tag{18}$$

Eq. (18) is to be supplemented with Eq. (16) to obtain the intensity perturbation from the refractive-index perturbation, and with Eq. (10) to obtain the phase perturbation from the intensity perturbation. This method allows relatively easy computation of all the dependent variables with closed-form expressions.

The initial conditions remain to be specified. For the blooming-induced refractive-index variations, $\delta n_B = 0$ and all its time derivatives are zero at $t = 0-$, for all ξ and all k. This merely restates the assumption that the laser does not heat the medium until it is turned on. At the ξ-boundary of the solution region, the value of $\xi = 0$ corresponds to the high-energy laser (HEL) transmitter location. At this boundary the initial conditions are specified and propagate up to ξ_{max}. At $\xi = 0$, and $\delta n_B(\xi = 0)$ and $\partial_\xi \delta n_B(\xi = 0)$ are determined by the intensity, and phase, respectively, of the HEL beam. The relations are as follows:

$$\delta n_B\,(\tau = 0) = \partial_\tau\, \delta n_B(\tau = 0) = \partial_\tau^2\, \delta n_B(\tau = 0) = 0. \tag{19a}$$

$$\left[\frac{\partial_\tau^2}{\mu^2} + 1 \right] \partial_\tau\, \delta n \,\Big|_{\xi=0} = - \frac{\delta I}{\beta}\Big|_{\xi=0} \tag{19b}$$

$$\left[\frac{\partial_\tau^2}{\mu^2} + 1 \right] \partial_\tau\, (\partial_\xi \delta n) \,\Big|_{\xi=0} = - \frac{\delta \phi}{\beta}\Big|_{\xi=0} \tag{19c}$$

These Eqs., (18), (16), (10), and (19) determine the evolution of the heated medium, for all times and positions provided the intensity perturbations remain small compared to I_0.

2.2 Intensity and Phase Variance

The above equations may be integrated numerically; however, this procedure for solution of partial differential equations may lead to instabilities and convergence difficulties. To avoid these problems, a useful technique is to apply Laplace or Fourier transforms to either the ξ-variable or the τ-variable. Since the τ operator is more complicated, more is to be gained by transforming it. Also, since the temporal behavior is believed to have an unstable (not periodic) behavior, the Laplace transform appears more suitable than the Fourier transform. Performing the Laplace transform with respect to τ in Eq. (18) leads to the following result:

$$\left[\left(\partial_\xi^2 + 1\right)\left[(s/\mu)^2+1\right] s+1\right] \delta n_B(k,\xi,s) = -\delta n_T(k,\xi,t=0)/s \tag{20}$$

Let

$$G(s) = \left[1+ \left((s/\mu)^2 + 1\right)^{-1} s^{-1}\right]^{1/2} \tag{21}$$

Then Eq. (20) may be rewritten as follows:

$$\left[\partial_\xi^2 + G(s)^2\right] \delta n_B = - \delta n_T(k,\xi,0)\ (G(s)^2-1)/s \tag{22}$$

This equation may be solved immediately:

$$\delta n_B = A \cos\ (G(s)\xi) + B\sin(G(s)\xi) - \int_0^\xi d\xi'\ \delta n_T(\xi',0)(G(s)^2-1)\ \frac{\sin(G(s)(\xi-\xi'))}{G(s)s} \tag{23a}$$

The constants A and B are determined by the initial conditions at ξ=0: From Eqs. (19), one obtains

$$\delta n_B(k,\xi=0,s) = - \delta I(k,\xi=0,s)(G(s)^2-1)/\beta = A \tag{23b}$$

$$\partial_\xi\ \delta n_B(k,\xi=0,s) = - \delta\phi(k,\xi=0,s)(G(s)^2-1)/\beta = B\ G(s) \tag{23c}$$

Eqs. (23a) - (23c) may be used to obtain the explicit expression for the heating-induced refractive index variations.

For the intensity perturbation, one may take the Laplace transform of Eq. (15) and solve:

$$\delta I(k,\xi,s) = -\beta\delta n_B/\left(G(s)^2-1\right) + 0. \tag{24a}$$

This last expression seems to ignore turbulence-only induced scintillations; this is not the case because as the heating rate tends to zero, both δn_B and $G(s)^2 - 1$ tend to zero also. Thus this expression is not defined in that limit. However, it will be seen that turbulence-induced scintillation is included at time zero.

A similar equation for $\delta\phi$ is derivable from Eq. (10):

$$\delta\phi\ (k,\xi,s) = \partial_\xi\ \delta I = -\beta\left[\partial_\xi\ \delta n_B\right] / \left(G(s)^2-1\right) \tag{24b}$$

Thus one may write the following for the spatio-temporal evolution of the Fourier components of the intensity and phase:

$$\begin{aligned}\delta I(k,\xi,s) \;=\; & \delta I(k,\xi=0,s)\cos(G(s)\xi) + \delta\phi\ (k,\xi=0,s)\sin\ (G(s)\xi)/G(s) \\ & + \beta\int_0^\xi d\xi'\ \sin\ (G(s)(\xi-\xi'))\ \delta n_T\ (\xi',0)/G(s)\ s\end{aligned} \tag{25a}$$

$$\begin{aligned}\delta\phi(k,\xi,s) \;=\; & -\delta I(k,\xi=0,s)\ G(s)\ \sin(G(s)\xi) + \delta\phi\ (k,\xi=0,s)\cos\ (G(s)\xi) \\ & + \beta\int_0^\xi d\xi'\ \cos\ (G(s)(\xi-\xi'))\ \delta n_T\ (\xi',0)/s\end{aligned} \tag{25b}$$

Note that Eq. (25a) has a turbulence-only induced scintillation term, that remains as the heating rate tends to zero and G(s) tends to one. Also note that the initial conditions of ξ=0 play an important role.

The second moments $\left\langle|\delta I(k,\xi,\tau)|^2\right\rangle$, $\left\langle|\delta\phi(k,\xi,\tau)|^2\right\rangle$, of the above random variables are of interest. For single pulse applications, it is assumed that the phase and intensity

fluctuations on the transmitted beam arise from atmospheric turbulence, the laser, and optical imperfections. These errors are assumed independent from one spatial frequency to the next, and the phase and intensity for a given frequency are also assumed independent. The aberrations are assumed constant over the duration of the pulse, and are band-limited white out to spatial frequency k_c, i.e.,

$$\left\langle |\delta I(k,0,s)|^2 \right\rangle = \begin{cases} \langle |\delta I_0|^2 \rangle / \pi k_c^2 s^2 & \text{for } |k| < k_c \\ 0 \quad \text{otherwise} \end{cases} \tag{26a}$$

$$\left\langle |\delta \phi(k,\xi=0,s)|^2 \right\rangle = \begin{cases} \langle |\delta \phi_0|^2 \rangle / \pi k_c^2 s^2 & \text{for } |k| < k_c \\ 0 \quad \text{otherwise} \end{cases} \tag{26b}$$

Finally, the turbulence-induced refractive index is assumed to obey

$$\left\langle \delta n_T(k,\xi_1,0)\, \delta \tilde{n}_T(k_2,\xi_2,0) \right\rangle = .033\, C_n^2 \left(k_{0T}^2 + k_1^2\right)^{-11/6} \exp\left(-(k_1/k_{in})^2\right)$$

$$\times\, \delta(\xi_1 - \xi_2) \left(\frac{k^2}{2k_0}\right) \delta(k_1 - k_2) \times \left(\frac{\pi}{2}\right) \tag{27}$$

The third-to-last factor of Eq. (27) is present because the delta function is a function of ξ, and not z. The last factor of $\pi/2$ is from the Markov approximation.

Thus taking the second moments of interest, one finds the following expressions:

$$\left\langle \delta I\,(k,\xi,\tau)|^2 \right\rangle = \frac{\left\langle |\delta I_0|^2 \right\rangle}{\pi k_c^2} \left| \int_{\varepsilon-i\infty}^{\varepsilon+i\infty} \frac{ds}{2\pi s} \cos(G(s)\xi)\, e^{s\tau} \right|^2$$

$$+ \frac{\left\langle |\delta\phi_0|^2 \right\rangle}{\pi k_c^2} \left| \int_{\varepsilon-i\infty}^{\varepsilon+i\infty} \frac{ds}{2\pi s} \frac{\sin(G(s)\xi)}{G(s)}\, e^{s\tau} \right|^2$$

$$+ \beta^2 \left(\frac{\pi}{4} \frac{k^2}{k_0}\right) \left(.033 \left(k_{0T}^2 + k^2\right)^{-11/6} \exp\left(-(k/k_{in})^2\right)\right)$$

$$\times \int_0^{\xi} d\xi'\, C_n^2 \left| \int_{\varepsilon-i\infty}^{\varepsilon+i\infty} e^{s\tau} \frac{ds}{2\pi s G(s)} \sin\left(G(s)(\xi-\xi')\right) \right|^2 \qquad (28)$$

$$\left\langle |\delta\phi\,(k,\xi,\tau)|^2 \right\rangle = \frac{\left\langle |\delta I_0|^2 \right\rangle}{\pi k_c^2} \left| \int_{\varepsilon-i\infty}^{\varepsilon+i\infty} \frac{ds}{2\pi s} G(s) \sin\left(G(s)\xi\right) e^{s\tau} \right|^2$$

$$+ \frac{\left\langle |\delta\phi_0|^2 \right\rangle}{\pi k_c^2} \left| \int_{\varepsilon-i\infty}^{\varepsilon+i\infty} \frac{ds}{2\pi s} \cos\left(G(s)\xi\right) e^{s\tau} \right|^2$$

$$+ \beta^2 \left(\frac{\pi}{4} \frac{k^2}{k_0}\right) \left(.033 \left(k_{0T}^2 + k^2\right)^{-11/6} \exp\left(-(k/k_{in})^2\right)\right)$$

$$\times \int_0^{\xi} d\xi'\, C_n^2 \left| \int_{\varepsilon-i\infty}^{\varepsilon+i\infty} \frac{ds}{2\pi s} \cos\left(G(s)(\xi-\xi')\right) e^{s\tau} \right|^2 \qquad (29)$$

The last term in Eqs. (28)-(29) yield the turbulence-only contribution for the blooming. In the limit as the heating rate goes to zero, G(s) tends to one, and in this limit the first two terms tend to the diffraction-only values, as does the turbulence contribution. The above are the equations used to compute the power spectral density of the phase and intensity, and thus the structure functions and the power-in-the-bucket.

2.3 Strehl Calculation

The expressions for the variances of the intensity and phase perturbations presented in the preceding section can be used to evaluate the farfield power spectral density of a finite aperture beam. By using an aperturing function, the farfield power can be obtained from the following equation:

$$P(\mathbf{x}) = \frac{\langle \left| \int \exp[\,\chi(\mathbf{x}') + i\phi(\mathbf{x}') + ik_o \mathbf{x}\cdot\mathbf{x}'/z\,]\, U(\mathbf{x}')\, d\mathbf{x}' \right|^2 \rangle}{\left| \int \exp(ik_o \mathbf{x}\cdot\mathbf{x}'/z)\, U(\mathbf{x}')\, d\mathbf{x}' \right|^2_{x=0}} \qquad (30)$$

where $U(\mathbf{x}')$ is the aperture window function and χ denotes the log-amplitude of the electric field. It should be noted that the use of an aperturing function to define the extent of the finite beam does not properly model such effects as whole beam acoustic relaxation and diffraction. However, for time scales and whole beam Fresnel numbers for which these effects are unimportant, this approximation should work quite well, as our results show.

If $U(\mathbf{x}')$ is set equal to $\frac{4}{\pi D^2}$, the denominator is just one. The numerator may be simplified by the use of structure functions:

$$P(\mathbf{x}) = \iint \exp(-D_\chi(\mathbf{x}'-\mathbf{x}'')/2 - D_\phi(\mathbf{x}'-\mathbf{x}'')/2 + ik_o \mathbf{x}\cdot(\mathbf{x}'-\mathbf{x}'')/z)\; U(\mathbf{x}')U(\mathbf{x}'')d\mathbf{x}'d\mathbf{x}'' \qquad (31)$$

where D_χ and D_ϕ are the structure functions of the log-amplitude and phase, resp. and

$$D_\chi(\Delta x) = 2\pi \int k\, dk\, (1-J_o(|k|\,|\Delta x|)\, \langle I^2 \rangle/4 \qquad (32)$$

$$D_{\phi}(\Delta x) = 2\pi \int k\, dk\, (1-J_0(|k|\,|\Delta x|)\, \langle \phi^2 \rangle \qquad (33)$$

where J_0 is the zero'th order Bessel function. For circular beams, the expression for the farfield power has circular symmetry and may be integrated with respect to the angular coordinate to yield power spectral density as a function of nearfield spatial scale size. It is this function that is used to compare the results from analytic theory and wave optics code simulations. In addition, the variances of the intensity and phase (see equations 28 and 29) will be compared directly.

3.0 COMPARISON OF ANALYTIC THEORY AND CODE SIMULATION

In order to test the applicability of the linearized analytic theory described in the previous section, results from this theory were compared to output from our fully non-linear wave optics propagation code, PHOTON. The first comparison involved the calculation of the power spectra of the variance of phase and intensity aberrations as a function of time. For this calculation, it was assumed that the input conditions consisted of small scale intensity aberrations imposed on a plane wave. These perturbations were formed from bandlimited Gaussian white noise with spatial scales between 0.5 and 10.0 cm and had a total variance of 0.001. For larger variances, difficulties arose in calculating the power spectra of the phase, since the severe small scale thermal blooming present for large input aberrations induced large phase differences between adjacent grid points in our computer simulations and the subsequent failure of our phase reconstruction routine. Increasing the number of grid points to eliminate this problem for large variances would have been computationally prohibitive. It should be noted, however, that the power spectra of the farfield spot is not subject to this limitation since it does not involve rely on phase reconstruction.

For the variance comparisons, the absorption and laser intensity were adjusted to yield an average heating rate of ~10^6 radians/sec, a rate chosen to provide significant thermal blooming within a 10 μsec pulse. A laser wavelength of 2.8 μ was used for this comparison. The propagation distance was 5 meters, yielding a diffraction zone of 0.37 cm over the path length.

Results for these run conditions are presented in Figures 1 and 2. Fig. 1 shows output from the beginning of the simulation and Fig. 2 contains output at 10 μsec into to simulation. In Fig. 1, the two minima in the power spectrum of the variance of the intensity indicate the range of the bandlimited white noise. By 10 μsec, the minimum at larger angle has shifted to a lower frequency reflecting the presence of acoustic relaxation at the smaller scales. Similar trends are seen in the plots of the phase variance. For both time slices, agreement between the linear analytic theory and the non-linear computer simulation is excellent leading us to conclude that the linear theory contains most of the important physics of transient thermal blooming and that non-linear effects are unimportant for conditions of interest. This is consistent with results obtained for steady-state thermal blooming in a separate theoretical effort at NERA.

Figures 3-5 contains results from a finite beam calculation. The following input conditions were used for this calculation. A laser operating at 10.6 μ with a flat-top intensity profile and beam diameter of 8 cm was assumed. Half of the laser energy was absorbed over a path length of 5 meters. The laser fluence was adjusted so that 10 radians of blooming occurred in 10 μsec. Bandlimited Gaussian noise between 0.5 and 8 cm with a variance of one percent was used as the source of initial intensity aberrations.

Plotted in Figures 3-5 are time resolved results for the angular dependence of the laser farfield spot. In Figure 3, the farfield of the laser before any blooming has occurred is plotted. The structure in the power spectrum is due to the finite beam size. The minimum occurring near 1×10^{-4} radians corresponds to the location of the edge of the central lobe of the farfield spot. After 10 μsec of laser operation, the power at large angles, which correspond to small spatial scales in the nearfield, has increased significantly, as shown in Figure 4. After 15 μsec, the signal at wide angles has increased by more than an order of magnitude over the unbloomed values and the beam Strehl ratio has fallen by 50 percent.

Agreement between analytic theory and computer simulation for the finite beam is quite good although not quite as good as for the infinite plane wave calculation. This is at least partly due to the fact that the analytic theory currently models whole beam effects by windowing a plane wave. This method cannot account for whole beam acoustic relaxation effects. One way in which this is evident in our calculations is the difference in the location of the minima of the power spectra for the analytic theory and simulation as time progresses and whole beam acoustic effects become more important.

The results from the comparison between analytic theory and code simulation indicate that our computer code accurately models the physics of transient thermal blooming. We feel confident that in the light of this validation, the code can be used for predicting the outcome of a laboratory scale thermal blooming experiment. The conceptual design of such an experiment is the subject of the next section.

4.0 DESIGNING A LABORATORY SCALE EXPERIMENT

The results from the analytic theory presented in the previous section provide a set of guidelines for designing a laboratory scale STBS experiment. In order to achieve measurable STBS at least 10 radians of blooming must occur over 10 - 30 μsec for laser systems with intensity variances on the order of one percent. The radians of blooming achieved during a laser pulse is defined by

$$\phi = \frac{2\pi}{\lambda} \frac{\beta_g (\gamma-1)}{c_s^2 \rho_0} (1 - e^{-\alpha L}) \int_0^{\tau_p} I dt \qquad (34)$$

where ϕ is the number of radians of blooming, λ is the laser wavelength, β_g is the Gladstone-Dale constant, γ is the ratio of specific heats, c_s is the speed of sound and ρ_0 is the density in the blooming medium. α is the absorption coefficient which is assumed to be a constant in the preceding expression, L is the propagation distance through the blooming medium, I is the laser intensity and τ_p is the pulse length.

Other conditions must also be met. The spatial scales of the aberrations must be larger than the acoustic relaxation distance for the laser pulse length, $d > v_a \tau_p$, where v_a is the speed of sound in the blooming medium. For scales where this condition is violated, steady state thermal blooming (STRS) rather than transient thermal blooming (STBS) is operable. In addition, the laser beam diameter must be significantly larger than the spatial scales of the aberrations if whole beam effects are not to complicate the interpretation of our results.

For the blooming medium, a relatively small absorption cross section is desirable so that an absorption depth on the order of several meters can be achieved. This requirement

translates into an absorption coefficient of approximately 0.1 - 0.5 m^{-1}. In addition, the molecular relaxation time for energy transfer from internal degrees of freedom to heating must be much shorter than the laser pulse length if any thermal blooming is to be observed.

For the LANL Meteor II laser as currently configured operating at 10.6 μ, the preceding conditions translate into the following system constraints. If roughly half of the laser energy is absorbed in the blooming cell, then the total laser fluence should be greater than 4.5 j/cm^2, assuming that air containing a few torr of a suitable CO_2 absorber is the blooming medium. Fluences of this level can be obtained if the beam diameter is decreased to approximately 8 cm in the blooming cell. This amount of focussing has already been obtained for other experiments involving the Meteor laser.

For the absorbing medium, a substance with a small absorption cross section at 10.6μ and a relaxation time of less than a tenth of the pulse length (less than 3 μsec) is required. A literature search was conducted in order to identify such a molecule. Many potential absorbers were found. Most of these were low molecular weight halocarbons such as C_2H_5Cl, $C_2H_4Cl_2$, CF_2HCl and CF_3CHCl_2, although ammonia is another possibility. As specific examples, let's choose the first two substances. In order to absorb half of the laser energy over a 5 meter path length, an absorption coefficient of 0.14 m^{-1} is needed. This can be obtained by using ~17 torr of chloroethane or ~6.5 torr of dichloroethane in an atmosphere of air. The vapor pressure of dichloroethane is considerably higher than 7 torr at room temperature and chloroethane is a gas.

Values for the V-T relaxation rates for these molecules were obtained from personnel at LANL and are ~2 ns/atm and ~5 nsec/atm for chloroethane and dichloroethane, resp. For the concentrations needed for the thermal blooming experiment, these rates correspond to relaxation times of 0.1 and 0.6 μsec, resp., neglecting any contribution to the V-T rate from air. If the V-T rates given above are those corresponding to the lowest vibrational level, the actual relaxation times will probably be somewhat slower since the absorption of CO_2 radiation will most likely populate a most highly excited vibrational level. However, if intramolecular V-V transfer is near gas kinetic (a not unreasonable assumption) and the laser energy corresponds to only a few vibrational quanta, then the relaxation time should still be in the acceptable range.

Two other uncertainties about the properties of the potential absorbers still remain. In general, small cross sections indicate absorption from excited vibrational states whose

population can be quite small at room temperature. The possibility therefore exists that the medium will bleach. In addition, several halocarbons are known multi-photon absorbers at high CO_2 flux levels. The potential absorbers that we have identified may be ones as well. If this were the case, the effective absorption depth might become too small to be useful for the proposed experiment. Both of these uncertainties could be resolved using a small absorption cell and a modest power CO_2 laser before the design of the actual thermal blooming experiment is finalized.

Meteor operating as an HF laser was also considered for a thermal blooming experiment. Predictions for the expected HF output power and spectral content for pumping conditions leading to a 10 - 30 μsec long pulse were obtained from personnel at Schafer Associates. The fluence levels of ≥ 5 j/cm^2 required for a successful thermal blooming experiment employing HF should be easily obtainable. However, the temporal dependence of the spectral output from the HF laser could greatly complicate the interpretation of the experiment results. Molecules usually have highly structured (i.e., vibrational) absorption profiles around 2.8μ. This structure, when coupled with the time varying output from the HF laser, would yield a time dependent absorption coefficient. If interest exists in pursuing an HF thermal blooming experiment, our analytic model and computer code could be modified to incorporate time varying absorption, but it increases the complexity of the problem.

5.0 EXPERIMENTAL SETUP

The experiment involves blooming of a medium by a laser pulse several tens of microseconds in length. The only means of diagnosing the transient blooming involves making time-resolved measurements of the scattering due to index of refraction inhomogeneities caused by the thermal blooming. It is possible to measure the time-resolved scattering of the IR heating beam using an array of discrete IR detectors such as HgCdTe detectors or using an IR-to-visible converter (Quantex, Sunstone) and visible detectors. This approach, measuring the effect of thermal blooming on distortions of the heating beam, was used by NERA in the steady-state thermal blooming experiment. However, the greater dynamic range of visible detectors and the relative ease of shuttering visible beams on microsecond timescales makes it preferable to diagnose the transient blooming with a visible beam that propagates through the blooming medium. The preferred configuration shutters the unexpanded visible beam with a fast, acousto-optic

shutter with microsecond time resolution and detects the far-field spot with a monolithic array of detectors such as a CCD. In order to improve rejection of the heating beam backscatter, the visible beam is preferably counterpropagating. The schematic optical layout is shown in Figure 6.

The heating beam, a 10.6μm beam from Meteor II, reflects off a mirror or a flat window. The flat is only partially reflecting and serves as a means of attenuating the beam by ~10×. Next, the beam reflects off a patterned reflector which serves as a fixed intensity modulator, i.e., a mirror with small holes drilled in it to produce a reflection with a non-uniform spatial pattern. The beam then passes through an NaCl wedge which serves as a beamsplitter and into the blooming cell. After exiting the cell, the beam passes through two more NaCl beamsplitters and into a beam dump. The second beam splitter reflects part of the main beam onto an IR camera or a set of discrete IR detectors. A counterpropagating HeNe beam is switched by a combination of mechanical and acousto-optic shutters. The beam is expanded, passed through an IR blocking glass flat, and is partially reflected into the beam train by another glass wedge and one of the NaCl beamsplitters. After passing through the blooming cell, the HeNe beam is reflected by a beamsplitter and a glass wedge, passed through an IR blocking glass flat. The beam is taken to the far-field by a lens, reduced in intensity by ND filters, and detected by a CCD camera.

5.1 Detailed Layout Description

The beamsplitters and windows of the blooming cell can be made of NaCl. 10cm NaCl windows are available off-the-shelf from Janos Technology and possibly other manufacturers with NaCl capability such as Optovac, Engelhard Corp., and others. Experience with Meteor optics should indicate whether special high damage threshold surface finishes need to be specified. With ~30' wedges, there should be no ambiguity of the front surface reflection and the rear surface reflection for the 1mrad field of view of interest. The optional blank used to attenuate the beam should have its rear surface AR coated for 10.6μm so that only the front surface reflects the beam.

An uncoated NaCl surface at 45° will reflect 1% of p-polarized and 9% of s-polarized 10.6μm or 633nm radiation. Thus, glass beam blocks are necessary to absorb any reflected 10.6μm radiation that would otherwise interfere with the diagnostic HeNe beam. The optical layout has each beam block in two parts. First, a glass wedge at 45° absorbs >85% of the beam. A second flat that is AR coated for the visible absorbs any

reflected 10.6μm radiation. The 10.6μm beam is attenuated in this two-step sequence in order to minimize the effect of heating on the 633nm beam quality. The bulk of the absorption takes place in a glass wedge off which the HeNe beam is reflected. The distortions of the surface are less than the OPD that would be impressed on a beam transmitted through the absorber. The second flat is included to ensure that 100% of the IR radiation is absorbed.

The patterned reflector serves as an intensity screen that imposes scintillations on the beam to seed the blooming interaction. If the laser intensity profile is sufficiently scintillated, this intensity screen is unnecessary. Assuming it is necessary, the pattern can be imposed by drilling a pseudo-random hole pattern. The hole size is chosen so that due to diffraction, the blooming cell cannot resolve the holes. If the screen is 2m from the cell, holes 4mm or smaller in diameter can be used.

The infrared detector array is used to measure the intensity variations of the heating beam, necessary for comparing experimental results with theory. These measurements should be made with no blooming medium present so as not to confuse the intensity variations of the laser and scintillations due to blooming. Ideally, this detector array will be able to make time resolved measurements of the Meteor beam intensity with ~100 gray levels or ~7 bits of dynamic range. This could be achieved by using discrete HgCdTe detectors and data acquisition electronics. If the IR beam is too intense after a single reflection off an NaCl flat, additional reflections off anti-reflection coated flats are necessary to reduce the beam intensity. An alternative is to use an IR array detector such as a Spiricon pyroelectric array. This array cannot be read out or gated during a laser pulse, so only integrated intensity profiles could be measured. With this sort of detector, some assumptions must be made regarding the time variation of the laser intensity. Some of these assumptions can be checked by varying the laser operating parameters and observing the change in the integrated intensity profile.

The HeNe laser is switched by a mechanical and an acousto-optic shutter. A fast mechanical shutter such as is available from Vincent Associates is necessary since the acousto-optic shutter has finite rejection during the off phase, typically less than 1000:1. Suitable acousto-optic shutters with sub-microsecond time resolution are available from Newport, IntraAction Corp., and a variety of other vendors. Note that with 1000:1 rejection, 2ms mechanical exposure time and 2μs acousto-optical exposure time, stray light during the time the acousto-optic shutter is closed is equal to the light when it is open.

Thus, careful calibration of the exposure with the acousto-optic shutter closed must be performed.

The HeNe beam is expanded from ~1mm diameter to ~100mm diameter. A high-quality beam must be maintained in order to preserve most of the dynamic range for the aberrations due to thermal blooming. This can be accomplished with a single, high quality beam expander with integral spatial filter such as the Tropel design available from Newport or another interferometrically tested design.

The blooming cell is a few meters in length and ~10cm in diameter. It is unavoidable that some thermal turbulence will be present due to fluctuations in the room temperature. However, recent experience with a steady-state thermal blooming experiment indicates that this disturbance can easily be measured and calibrated as long as it does not vary on short time scales.

Even after four 9% reflections and ~2μs exposures, the HeNe beam may be too bright for a sensitive detector and will need attenuation. A 20mW laser with 5ms exposures required $10^{7\text{-}9}\times$ attenuation in NERA's steady-state blooming experiment. If a similar laser, detector, and f/# far-field lens are used, attenuation of $10^{0\text{-}2}\times$ will be required. Neutral density filters placed near the focal plane can attenuate the beam without significant distortion.

The HeNe detector is preferably a monolithic array such as a CCD detector. The detector array should have as large a dynamic range as possible. The power in ring plots exemplified by Figures 3-5 typically have useful information over two decades which corresponds to three decades or so in the intensity. Commercially available cooled CCD cameras from Photometrics, Ltd. and possibly other vendors readily achieve 12-bits of useful dynamic range. The camera should have a mechanical shutter to screen out stray light. This camera should also be capable of delayed readout to minimize electromagnetic interference from the laser pulse on the readout electronics.

An array with at least 128x128 pixels should be more than sufficient to resolve the angular structure of interest. Note that to match the diffraction spot size to a camera pixel of $\sim(20\mu m)^2$, the far-field lens will have to be ~f/40. If the resulting 4m focal length is unacceptable, an f/5-10 lens with a subsequent magnification with a high-quality microscope objective will work. Note that a diffraction-limited achromat is sufficient for

the far-field lens since it will only be used over a narrow field of view at infinite conjugate. If a large f/# lens is used, a simple lens will suffice.

5.2 Experimental Protocol

A set of experiments that will quantify intrapulse blooming and that can be compared to theory are given in the following paragraphs. Note that careful photometry assumes that CCD bias frames, flat field frames, and dark frames (without the laser on) are taken so that dark and bias values can be subtracted and the detector non-uniformity can be corrected:

1. Measure the IR intensity of the heating laser pulse with no blooming medium present in order to calibrate the spatial intensity fluctuations in the heating beam. If the IR detector is a monolithic array with poor time resolution, take frames with different laser operating parameters and infer the instantaneous spatial statistics. Make measurements for a series of pulses in order to determine the variation from one laser pulse to the next.

2. Measure the HeNe intensity at $t=-\Delta t$ (before the IR laser fires) and at $t=0$ for a set of laser pulses in order to determine whether transient effects are causing spurious data and to calibrate the noise levels.

3. Measure the HeNe intensity at $t=-\Delta t$ (before the IR laser fires), $t=2\mu s$, and at $t=10\mu s$ for a set of laser pulses in order to determine whether the data are repeatable and with what confidence. This must be done because subsequent measurement of the temporal variation will use different laser shots and their consistency must be ascertained. If significant variations occur, try and correlate them with the IR laser intensity measurements made with each pulse. If significant variations occur and do not correlate well with the IR laser measurements, the approach of measuring temporal variation with different laser shots will not work and a significantly more complicated detector, either a streak camera or a discrete array of fast photodetectors, must be employed to obtain time resolved measurements of a single laser shot.

4. For a fixed power level, measure the HeNe profile at $t=-\Delta t$ and at $t=n\Delta t$ for $n=0,1,2\ldots$, i.e., resolve the temporal behavior for a fixed power level.

5. Measure the HeNe profile at t=-Δt , t=2μs, and at t=10μs for two different laser energies, the second being obtained by replacing the 45° mirror immediately after the laser with a partially reflecting flat. This experiment will determine the scaling of the blooming effect as a function of laser power for a fixed time into the pulse.

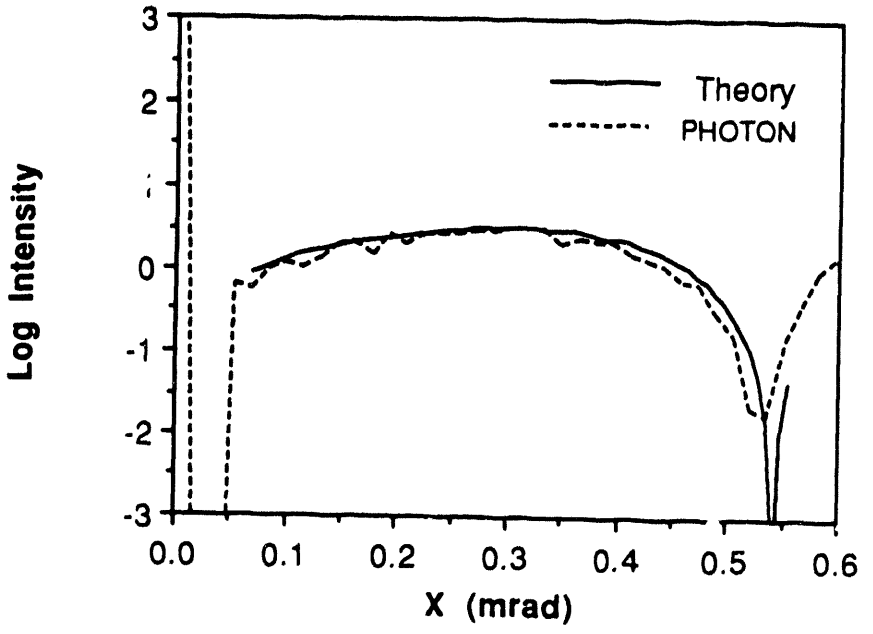

Figure 1a: Frequency dependence of the variance of the intensity before blooming occurs.

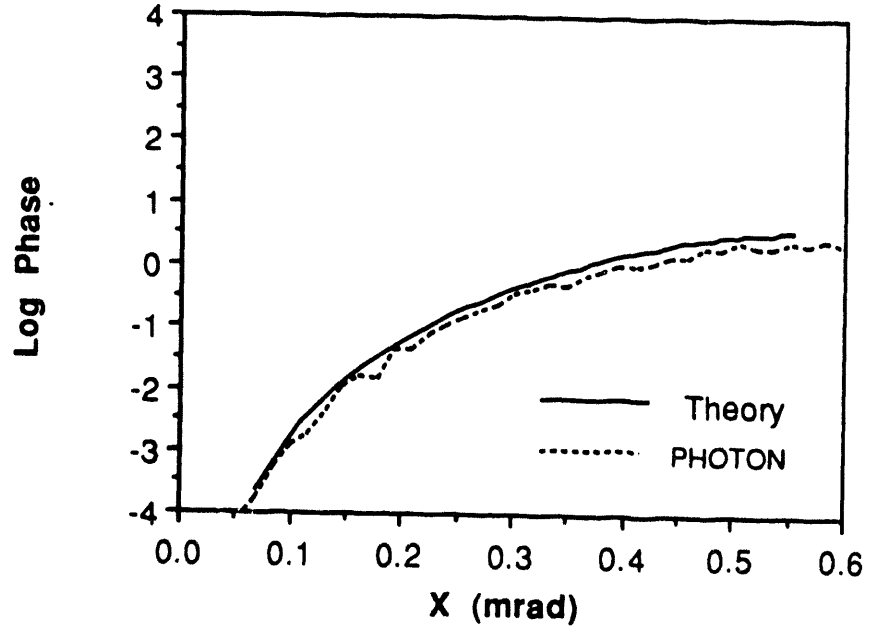

Figure 1b: Power spectrum of the phase variance at the beginning of the blooming run.

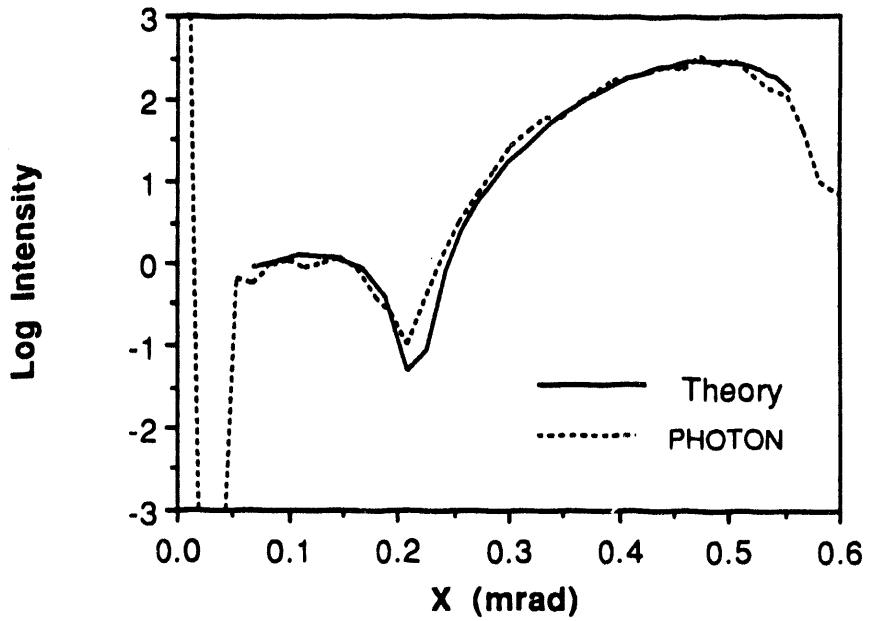

Figure 2a: Frequency dependence of the intensity variance 10 μsec into pulse. The time dependence of theminimum in the variance is due to acoustic relaxation of small spatial scales.

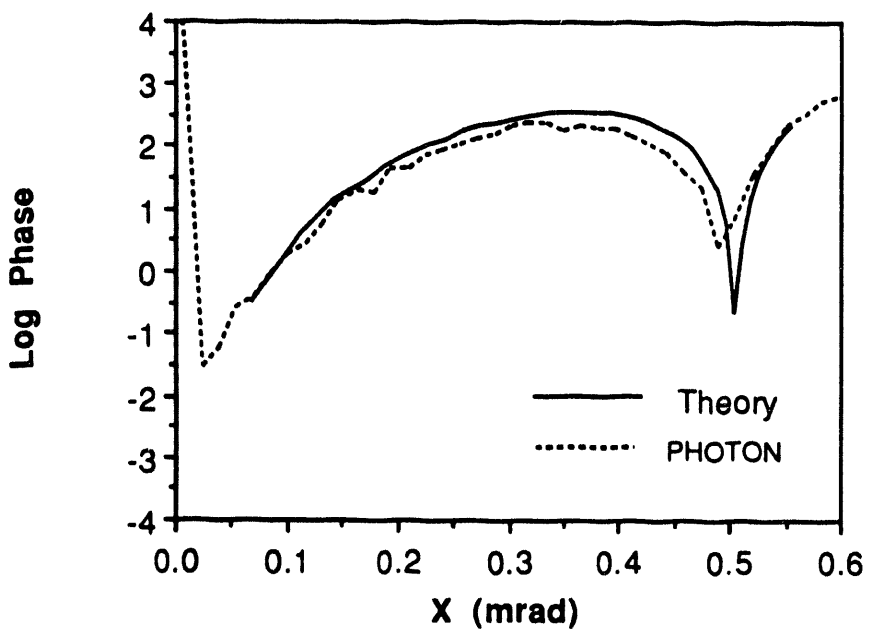

Figure 2b: Frequency dependence of the phase variance after 10 μsec.

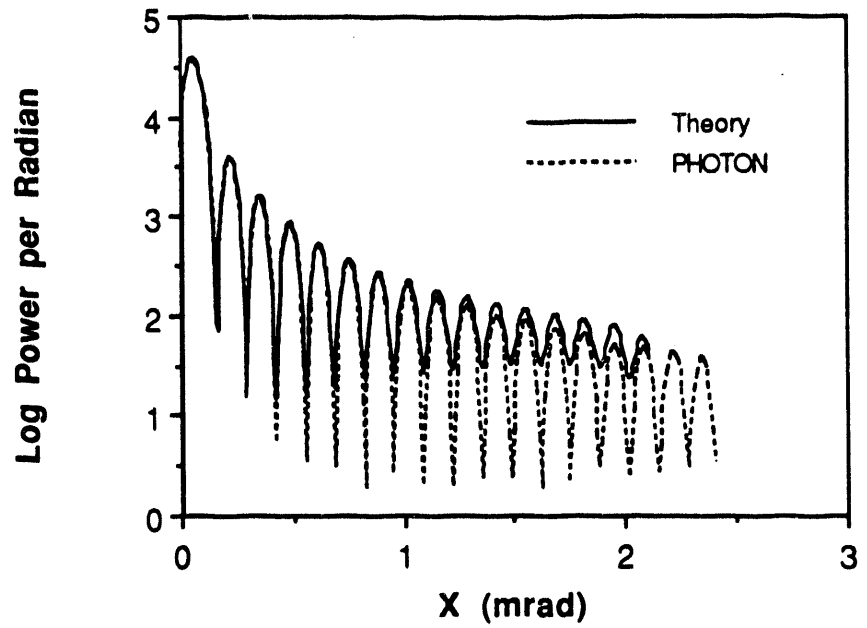

Figure 3: Angular dependence of laser farfield spot prior to blooming. Structure in spectrum is due to finite beam dimensions.

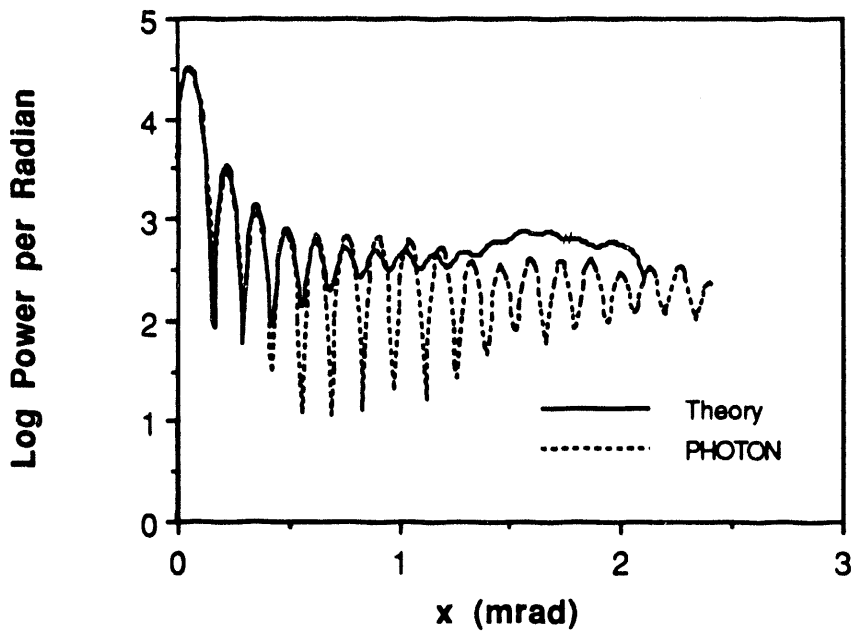

Figure 4: Power spectrum of laser farfield spot 10 μsec into the run.

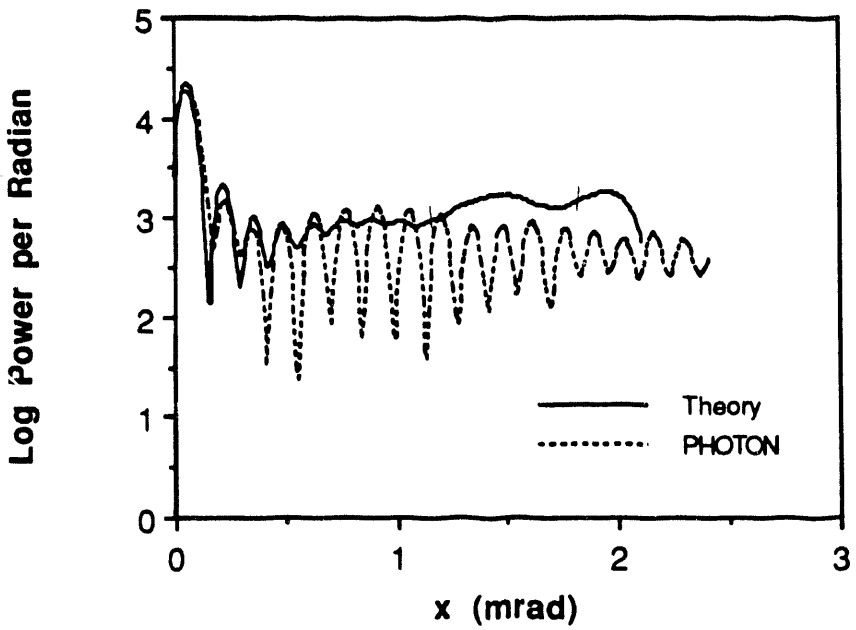

Figure 5: Power spectrum of laser farfield spot after 15 μsec.

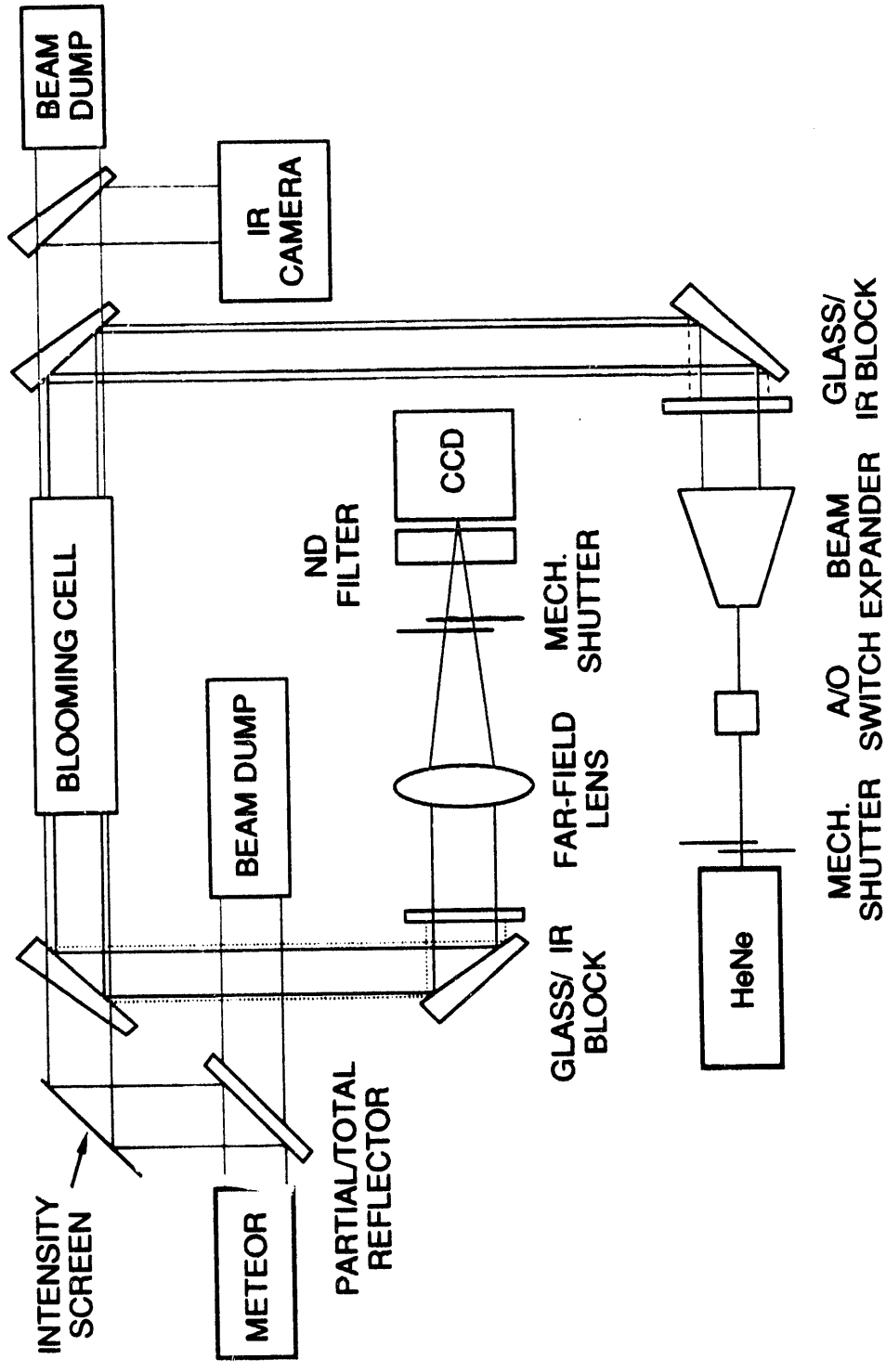

Figure 6: Schematic layout of the intrapulse blooming experiment

DATE
FILMED
8/31/94

END